Batteries & Supercaps

Research Article
doi.org/10.1002/batt.202300187

Chemistry Europe
European Chemical Societies Publishing

www.batteries-supercaps.org

In situ Formation of Solid Electrolyte during Lithiation Process of $MgCl_2$ Anode in an All-Solid-State Lithium Battery

Atsushi Inoishi,*[a] Miyuki Suyama,[a] Eiichi Kobayashi,[b] Shigeto Okada,[c] and Hikari Sakaebe[a]

All-solid-state lithium batteries, which are free from the risk of liquid entanglement, are expected to have high energy densities and high safety. In this study, the omission of a solid electrolyte from the electrode and an increase in thickness of the electrode were investigated to improve the energy density of all-solid-state lithium batteries. We focused on $MgCl_2$, which reversibly self-generates a solid electrolyte during the lithiation process, as an anode material that can operate without a solid electrolyte incorporated into the electrode mixture. Indeed, the electrochemical properties of the $MgCl_2$ electrode were approximately the same with or without a pre-contained solid electrolyte, $LiBH_4$. X-ray diffraction and X-ray absorption spectroscopy analyses showed that lithiation produced Mg and LiCl, which were recovered to $MgCl_2$ by subsequent delithiation. The available electrode thickness was also investigated, and the thickness limit for the first lithiation was found to be ~100 μm.

Introduction

All-solid-state lithium batteries have attracted intensive attention because they can provide high energy density and safety.[1–3] In recent years, oxide-and sulfide-based electrolytes have been the electrolytes mainly considered for use in solid-state batteries.[4–7] However, hydride-based electrolytes, which exhibit high ionic conductivity and high compatibility with metallic lithium anodes, are feasible alternatives.[8–14] To achieve high capacity in these solid-state lithium-ion batteries, it is first necessary to remove as much of the solid electrolyte and conductive carbon contained in the electrode as possible. In addition, in the case of conventional mixing, electrodes and electrolytes only make contact at the macroscale, which leads to high interfacial resistance. Recently, we reported all-solid-state lithium batteries that operate via electrochemical lithium insertion into some anode materials. We first investigated $Mg(BH_4)_2$, which showed a suitable operating voltage and a large lithiation capacity: 0.9 V vs. Li/Li^+ and 751 mAh g^{-1}, respectively.[15] We also recently investigated MgH_2 as an anode material, which also showed a suitable operating voltage of 0.5 V vs. Li/Li^+ and a large capacity of 1818 mAh g^{-1}.[16] The following electrochemical reactions are associated with the insertion of Li^+ into $Mg(BH_4)_2$ and MgH_2:

$$Mg(BH_4)_2 + 2\,Li^+ + 2\,e^- \rightarrow 2\,LiBH_4 + Mg \quad (1)$$

$$MgH_2 + 2\,Li^+ + 2\,e^- \rightarrow 2\,LiH + Mg \quad (2)$$

In these conversion-type electrodes, $LiBH_4$ and LiH are generated as lithium salts during lithiation, and ionic conduction paths are formed during the electrochemical reaction. Surprisingly, a solid electrolyte is not required in these electrode mixtures and reasonable battery performance was achieved with an electrode composed of active material (i.e., $Mg(BH_4)_2$ or MgH_2) and acetylene black (AB), without an electrolyte powder. We refer to this new concept as the "in situ formation of solid electrolyte," which directly contributes to an increase in capacity for the anode. In the present study, we focus on $MgCl_2$ as a new anode active material. $MgCl_2$ has rarely been applied as an anode material. In the case of $MgCl_2$, the following electrochemical reaction is assumed to occur upon insertion of Li^+:

$$MgCl_2 + 2Li^+ + 2e^- \rightarrow 2LiCl + Mg \quad (3)$$

If the ionic conductivity of LiCl is sufficiently high, it should be available as an anode material capable of *in situ* formation of a solid electrolyte (Figure 1). Initially, the formation of LiCl and Mg will proceed from the interface between the solid electrolyte layer and the electrode mixture, and the electrode reaction will proceed toward the current collector through the LiCl for the ionic conduction pathway. The theoretical capacity for $MgCl_2$ is 562 mAh g^{-1}, which is much higher than the theoretical capacities for conventional anode materials such as graphite and $Li_4Ti_5O_{12}$. In addition, $MgCl_2$ is a safe and low-cost material.

[a] Dr. A. Inoishi, M. Suyama, Prof. H. Sakaebe
Institute for Materials Chemistry and Engineering
Kyushu University
6-1 Kasuga-koen, Kasuga-Shi 816-8580 (Japan)
E-mail: inoishi@cm.kyushu-u.ac.jp

[b] Dr. E. Kobayashi
Kyushu Synchrotron Light Research Center
8-1 Yanagigaoka, Tosu-shi, Saga 841-0005 (Japan)

[c] Prof. S. Okada
Transdisciplinary Research and Education Center for Green Technology
Kyushu University
6-1 Kasuga-koen, Kasuga-Shi 816-8580 (Japan)

Supporting information for this article is available on the WWW under https://doi.org/10.1002/batt.202300187

Research Article
doi.org/10.1002/batt.202300187
Chemistry Europe
European Chemical Societies Publishing

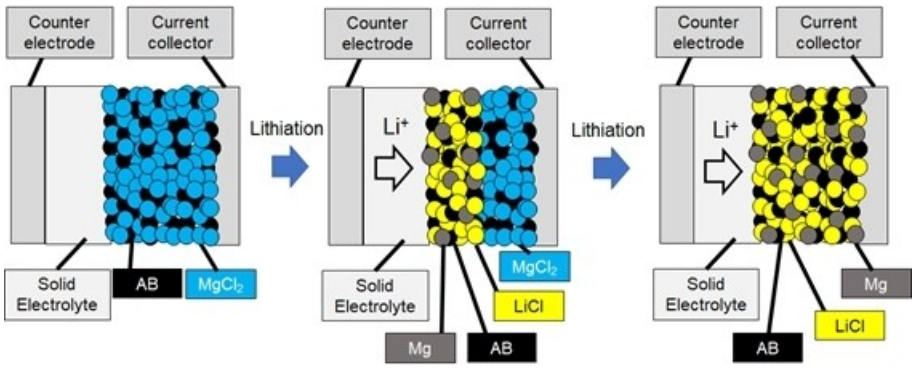

Figure 1. Schematics of electrochemical reaction for solid-state battery with $MgCl_2$ electrode.

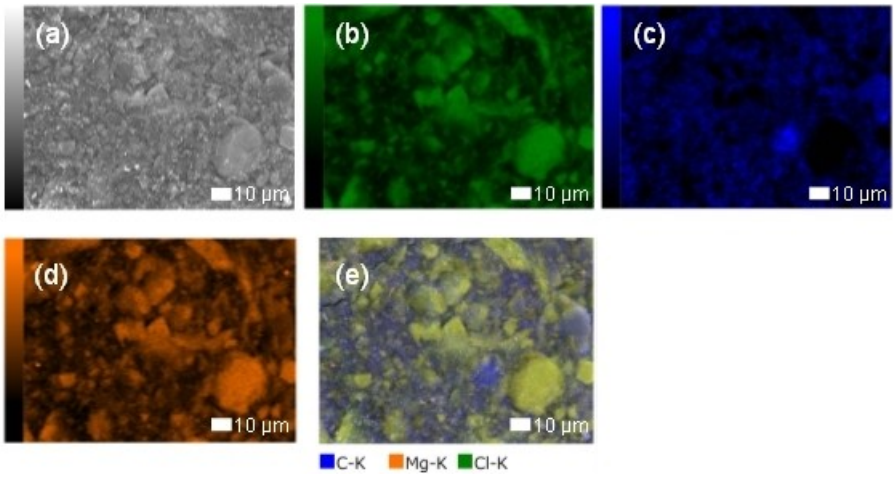

Figure 2. a) SEM image of $MgCl_2$-based electrode mixture and mapping images for b) Cl, c) C, d) Mg, and d) combined elements. The pellet was prepared by compaction at 380 MPa at room temperature.

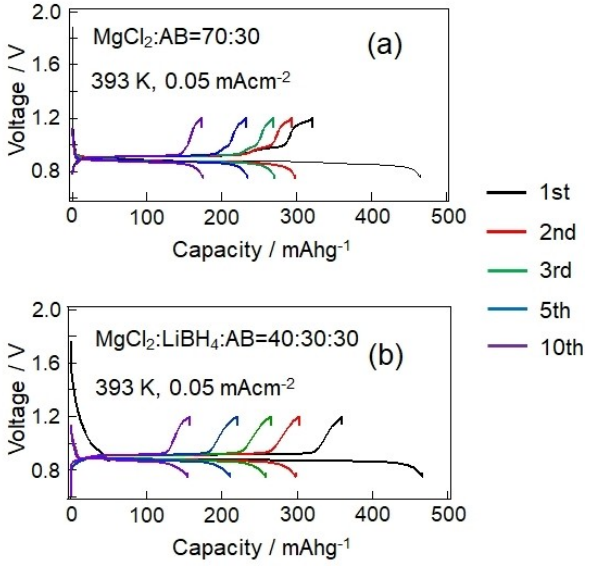

Figure 3. a) Discharge-charge curves for $Li/LiBH_4/MgCl_2$ cell without $LiBH_4$ in the electrode mixture. b) Discharge-charge curves for $Li/LiBH_4/MgCl_2$ cell with $LiBH_4$ in the electrode mixture.

Here, we investigated the *in situ* electrochemical formation of a lithium-ionic conduction path from $MgCl_2$ and evaluated the redox mechanism for $MgCl_2$.

Results and Discussion

To investigate the morphology of the pressed electrodes, we conducted scanning electron microscopy (SEM) observations. Figure 2(a) shows an SEM image of the $MgCl_2$-based electrode mixture (electrode 2). Mapping images for Cl, C, and Mg are shown in Figure 2(b), (c), and (d), respectively. Figure 2(e) shows the combined map. Before the observation, the powder was pressed at 380 MPa, which was the same pressure used when fabricating the solid-state batteries. A highly dense morphology was confirmed; therefore, the $MgCl_2$ electrode exhibited high plasticity. The particle size of $MgCl_2$ was from 1 to 30 μm. Figure 3(a and b) shows discharge-charge curves for $Li/LiBH_4/MgCl_2$ cells with $LiBH_4$ (electrode 1) and without $LiBH_4$ (electrode 2) in the electrode mixture, respectively. For

Research Article
doi.org/10.1002/batt.202300187
Chemistry Europe
European Chemical Societies Publishing

electrode 1, the initial lithiation and delithiation capacities were 465 and 321 mAh g^{-1}, respectively. The initial lithiation capacity was 82% of the theoretical capacity for $MgCl_2$. However, in the case of electrode 2, the initial lithiation and delithiation capacities were 465 and 359 mAh g^{-1}, respectively. The initial lithiation capacity for electrode 2 was also 82% of the theoretical capacity for $MgCl_2$. Therefore, the presence of $LiBH_4$ in the electrode does not drastically affect the initial lithiation capacity, indicating that the lithium conduction path is formed from $MgCl_2$ by the electrochemical reaction. However, the first delithiation capacity for electrode 1 was larger than that for electrode 2, possibly because the ionic conduction pathway in electrode 2 was not sufficiently established during the initial lithiation process to enable the recovery of Mg to $MgCl_2$. However, the lithiation capacities for electrodes 1 and 2 at the 10th cycle were 154 and 174 mAh g^{-1}, respectively. Therefore, electrode 2 exhibited better cycle stability, indicating that the ionic conducting pathway did not seriously affect degradation. Other possible reasons for the degradation include a volume change of the electrode, a change in the particle size, a change in the electrode's electronic conduction properties, or the occurrence of a side reaction between the $LiBH_4$ and $MgCl_2$. Figure 4 shows XRD patterns for the $MgCl_2$ electrode (without $LiBH_4$ electrolyte) before and after the discharge-charge measurement. The pattern for the electrode mixture shows diffraction peaks attributable to $MgCl_2$. Therefore, after ball-milling with AB, the structure of $MgCl_2$ was retained. After lithiation, weak peaks due to $MgCl_2$ were still observed but peaks associated with metallic Mg appeared. After delithiation, the peaks for metallic Mg decreased in intensity; however, the peaks for $MgCl_2$ were no longer observed. Therefore, we assumed that $MgCl_2$ was generated in a low-crystallinity state after delithiation. For the two samples (after lithiation and after delithiation), the position and intensity of the peaks for $LiBH_4$ differed, likely as a result of a change in the crystal structure of $LiBH_4$, although details of the mechanism are unclear. After lithiation, no peak at about 25°, associated with a low-temperature $LiBH_4$ phase,[17] was observed. Although the reason for this is as yet unknown, possible factors include pressure, temperature, and side reactions with the active material. Figure 5(a) shows Mg K-edge X-ray adsorption spectra for the $MgCl_2$ electrode (without $LiBH_4$ electrolyte, electrode 2) before and after the discharge-charge measurement. The spectrum of

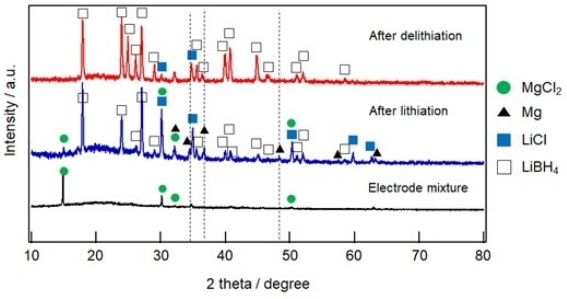

Figure 4. XRD patterns for $MgCl_2$ electrode before and after discharge-charge measurement.

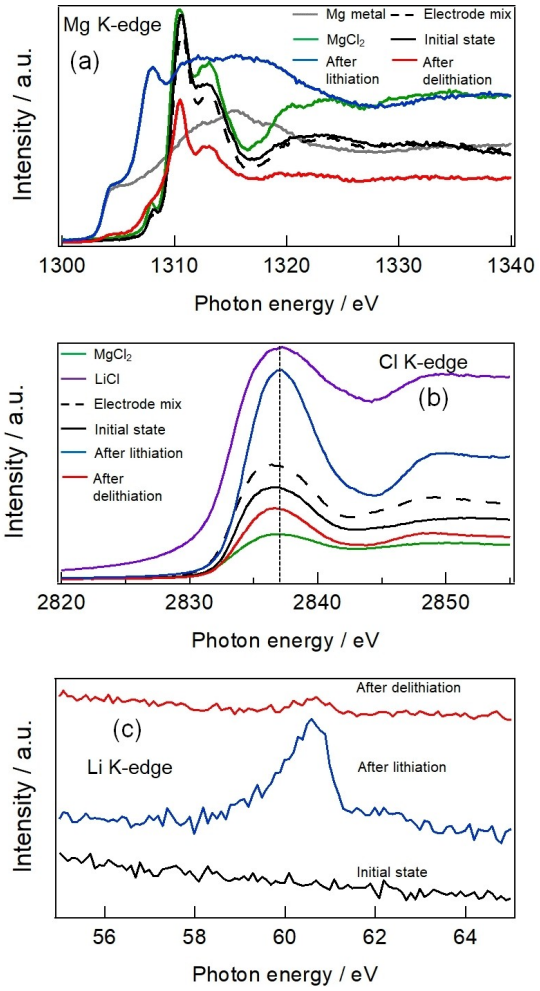

Figure 5. X-ray adsorption spectra of $MgCl_2$ electrode before and after discharge–charge measurement: a) Mg K-edge, b) Cl K-edge, and c) Li K-edge. The $MgCl_2$ electrode thickness in the solid-state battery was 50 μm.

$MgCl_2$ shows a sharp peak at 1310 eV. The "initial state" corresponds to the $MgCl_2$ electrode before the discharge–charge measurement, but after the cell was fabricated and heated to the measurement temperature (393 K). This spectrum is similar to those of the electrode mixture and $MgCl_2$, indicating that the initial state is still $MgCl_2$. After the initial lithiation, a new adsorption peak at 1302 eV was observed. This peak has been observed in the spectrum of metallic Mg.[18,19] Therefore, $MgCl_2$ is reduced to metallic Mg during the lithiation process. After the subsequent delithiation, a spectrum similar to that for the initial state was observed, indicating that $MgCl_2$ is reversibly formed after the delithiation process. Figure 5(b) shows Cl K-edge X-ray adsorption spectra for the $MgCl_2$ electrode (without $LiBH_4$ electrolyte, electrode 2) before and after the discharge-charge measurement. The spectra for the initial state and the delithiated state are similar to the spectrum of $MgCl_2$. After lithiation, the main intense peak was slightly shifted to higher energy, which corresponds to the adsorption observed in the spectrum of LiCl.[20] Figure 5(c) shows Li K-edge X-ray adsorption spectra for the $MgCl_2$ electrode (without $LiBH_4$ electrolyte, electrode 2) before and after the discharge–charge

Research Article
doi.org/10.1002/batt.202300187

measurement. After lithiation, an adsorption peak due to LiCl was observed at 61 eV. This value and the features of the spectrum agree well with those reported previously.[21] The spectrum of the delithiated state also showed a small peak at the same position, indicating that some LiCl remained at the current-collector side after delithiation. The observed capacity indicates that 16% of the LiCl produced in the first lithiation remained after delithiation. These results confirm that LiCl plays a role in the *in situ* electrochemical formation of a lithium ionic conduction path in the $MgCl_2$ anode. We therefore measured the electrical conductivity of the LiCl. The LiCl powder was pressed at 380 MPa into a 10 mm diameter pellet, and Pt electrodes were sputtered onto the top and bottom surfaces. Figure S1 shows the electrical conductivity of the LiCl. At 393 K, which is the operating temperature of the battery in the present study, the electrical conductivity was 5.9×10^{-5} S cm^{-1}. This value indicates that LiCl exhibits sufficient conductivity to provide an ionic conduction path. Therefore, LiCl is a reasonable material for the *in situ* electrochemical formation of a lithium ionic conduction path in an $MgCl_2$ anode. The effects of the electrode thickness and current density on the discharge–charge characteristics were further investigated. In the analyses shown in Figure 3(a), a 50 μm-thick $MgCl_2$ electrode was used. Figure S2 shows discharge–charge curves for the Li/$LiBH_4$/$MgCl_2$ cells with thicker electrodes. In these cells, the electrode mixture does not contain the $LiBH_4$ electrolyte. When the electrode thickness is 180 μm, the initial lithiation and delithiation capacities were 297 mAh g^{-1} and 106 mAh g^{-1}, respectively. In this case, the overpotential was clearly increased. The lithiation capacity decreases (from 1st to 2nd) and then increases (from 2nd to 5th). In contrast, the lithiation capacity keeps decreasing in Figure 3(a). It is assumed that the long-distance movement of Li ions is difficult, and therefore the area of the conversion reaction gradually expands during early cycles for the case of a thick electrode. Figure 6 shows the initial lithiation capacity as a function of the electrode thickness for the $MgCl_2$ anode. The capacity increased linearly until the electrode thickness reached 100 μm but did not change beyond that. Therefore, we assumed that the first lithiation did not progress to a region thicker than 100 μm. Ohno *et al.* investigated the ionic and electronic resistance of ball-milled composite electrodes of lithium argyrodite (Li_6PS_5Cl) and carbon. They found that both the ionic and electronic resistance increased linearly with increasing electrode thickness. Therefore, the resistance of the electrode in our study is reasonably expected to also increase with increasing electrode thickness.[21] Figure S3 shows XRD patterns for the $MgCl_2$ electrode after the initial lithiation. When a thin electrode (50 μm) was used, metallic Mg formed (Figure 4). However, when a thick electrode (180 μm) was used, only peaks associated with $MgCl_2$ were observed. These results indicate that the current-collector side in the thick electrode was not lithiated. Figure S4 shows discharge–charge curves at a higher current density (0.5 mA cm^{-2}) for the Li/$LiBH_4$/$MgCl_2$ cell without $LiBH_4$ (electrode 2) in the electrode mixture. The electrode thickness was 50 μm, and the initial lithiation and delithiation capacities were 128 mAh g^{-1} (22% of theoretical capacity) and 59 mAh g^{-1}, respectively. These values are much smaller than those associated with the lower current density of 0.05 mA cm^{-2}. In our previous report on MgH_2 electrodes, the initial lithiation capacity was 1818 mAh g^{-1} (89% of theoretical capacity) at 0.5 mA cm^{-2}.[16] The utilization efficiency for MgH_2 is much greater than that for $MgCl_2$ at a high current density (0.5 mA cm^{-2}). In the case of MgH_2, the formed lithium salt is LiH, which exhibits a low conductivity of 10^{-7} S cm^{-1} at 393 K.[23] This conductivity is much lower than that of LiCl, which is formed by lithiation of $MgCl_2$. Therefore, the conductivity of the formed lithium salt is not the sole factor responsible for the high lithiation capacity and low overpotential. As another factor, we considered the different volumetric ratio for the Mg and lithium salts after lithiation (LiCl:Mg = 2.89:1, LiH:Mg = 1.39:1). The volume of metallic magnesium after lithiation of MgH_2 is much larger than that for $MgCl_2$, which leads to highly effective electronic conductivity in the MgH_2-based electrode. To fully understand the electrochemical properties of the *in situ*-formed solid electrolytes, other factors such as morphological changes and effective electronic conductivity should also be considered.

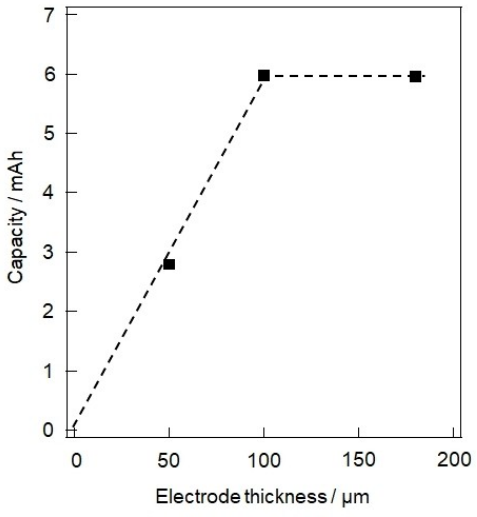

Figure 6. Initial lithiation capacity as a function of the electrode thickness of the $MgCl_2$ anode.

Conclusions

This work demonstrated for the first time the *in situ* formation of an ionic conducting path upon lithiation of $MgCl_2$. The electrochemical performance of the cell without $LiBH_4$ in the electrode mixture was similar to that of the cell containing a $LiBH_4$ electrolyte. XRD and XAS analyses indicated that LiCl and Mg were formed via lithiation and reversibly returned to $MgCl_2$ upon delithiation. The *in situ*-formed LiCl contributed to the superior electrochemical performance of the conversion reaction without an electrolyte in the electrode mixture. The available electrode thickness limit for the first lithiation was ~100 μm. This useful concept of *in situ* formation of a solid

electrolyte can increase the energy density of all-solid-state batteries. Overall, the concept works well for the first lithiation, but not for subsequent delithiation. It is necessary to optimize the powder particle size and the volumetric ratio in order to achieve good ionic and electronic conducting pathways.

Supporting Information

The authors have cited additional references within the Supporting Information [24–27].

Acknowledgements

This work was supported by JSPS KAKENHI Grant Numbers JP22H04621, JP20H05297 (Grants-in-Aid for Scientific Research on Innovative Areas "Interface IONICS") and JP21K05243. Part of this work was performed at the BL2 A beamline of the UVSOR Synchrotron Facility, Institute for Molecular Science (IMS program 22IMS6668). Part of this work was performed at the BL12 of the SAGA Light Source (Proposal No. 221118F).

Conflict of Interests

The authors declare no conflict of interest.

Data Availability Statement

The data that support the findings of this study are available from the corresponding author upon reasonable request.

Keywords: solid-state batteries · in-situ formation of solid electrolyte · $MgCl_2$

[1] J. Liu, H. Yuan, H. Liu, C. Zhao, Y. Lu, X. Cheng, J. Huang, Q. Zhang, *Adv. Energy Mater.* **2022**, *12*, 2100748.
[2] Y. Tian, G. Zeng, A. Rutt, T. Shi, H. Kim, J. Wang, J. Koettgen, Y. Sun, B. Ouyang, T. Chen, Z. Lun, Z. Rong, K. Persson, G. Ceder, *Chem. Rev.* **2021**, *121*, 1623–1669.
[3] L. Fan, H. He, C. Nan, *Nat. Rev. Mater.* **2021**, *6*, 1003–1019.
[4] R. Murugan, V. Thangadurai, W. Weppner, *Angew. Chem. Int. Ed.* **2007**, *46*, 7776–7781.
[5] H. Aono, N. Imanaka, G. Adachi, *Acc. Chem. Res.* **1994**, *27*, 265–270.
[6] Y. Seino, T. Ota, K. Takada, A. Hayashi, M. Tatsumisago, *Energy Environ. Sci.* **2014**, *7*, 627–631.
[7] N. Kayama, K. Homma, Y. Yamakawa, M. Hirayama, R. Kanno, M. Yonemura, T. Kamiyama, Y. Kato, S. Hama, K. Kawamoto, A. Mitsui, *Nat. Mater.* **2011**, *10*, 682–686.
[8] K. Kisu, S. Kim, H. Oguchi, N. Toyama, S. Orimo, *J. Power Sources* **2019**, *436*, 226821.
[9] S. Kim, H. Oguchi, N. Toyama, T. Sato, S. Takagi, T. Otomo, D. Arunkmar, N. Kuwata, J. Kawamura, S. Orimo, *Nat. Commun.* **2019**, *10*, 1081.
[10] L. Zeng, K. Kawahito, S. Ikeda, T. Ichikawa, H. Miyaoka, Y. Kojima, *Chem. Commun.* **2015**, *51*, 9773–9776.
[11] S. Ikeda, T. Ichikawa, K. Kawahito, K. Hirabayashi, H. Miyaoka, Y. Kojima, *Chem. Commun.* **2013**, *49*, 7174–7176.
[12] L. Zeng, T. Ichikawa, K. Kawahito, H. Miyaoka, Y. Kojima, *ACS Appl. Mater. Interfaces* **2017**, *9*, 2261–2266.
[13] L. Huang, L. Aymard, J. Bonnet, *J. Mater. Chem. A* **2015**, *3*, 15091–15096.
[14] A. E. Kharbachi, H. Uesato, H. Kawai, S. Wenner, H. Miyaoka, M. H. Sørby, H. Fjellvåg, T. Ichikawa, B. C. Hauback, *RSC Adv.* **2018**, *8*, 23468–23474.
[15] H. Sato, R. Sakamoto, H. Minami, H. Izumi, K. Ideta, A. Inoishi, S. Okada, *Chem. Commun.* **2021**, *57*, 2605–2608.
[16] A. Inoishi, H. Sato, Y. Chen, H. Saito, R. Sakamoto, H. Sakaebe, S. Okada, *RSC Adv.* **2022**, *12*, 10749–10754.
[17] H. Maekawa, M. Matsuo, H. Takamura, M. Ando, Y. Noda, T. Karahashi, S. Orimo, *J. Am. Chem. Soc.* **2009**, *42*, 894–895.
[18] J. W. Chiou, H. M. Tsai, C. W. Pao, K. P. Krishna Kumar, S. C. Ray, F. Z. Chien, W. F. Pong, *App. Phys. Lett.* **2006**, *89*, 043121.
[19] K. Witte, C. Streeck, I. Mantouvalou, S. A. Suchkova, H. Lokstein, D. Grötzsch, W. Martyanov, J. Weser, B. Kanngießer, B. Beckhoff, H. Stiel, *J. Phys. Chem. B* **2016**, *120*, 11619–11627.
[20] H. S. Lee, X. Q. Yang, J. McBreen, L. S. Choi, Y. Okamoto, *J. Electrochem. Soc.* **1996**, *143*, 3825–3829.
[21] S. Roychoudhury, Z. Zhuo, R. Quao, L. Wan, Y. Liang, F. Pan, Y. Chuang, D. Prendergast, W. Yang, *ACS Appl. Mater. Interfaces* **2021**, *13*, 45488–45495.
[22] S. Ohno, C. Rosenbach, G. F. Dewald, J. Janek, W. G. Zeier, *Adv. Funct. Mater.* **2021**, *31*, 2010620.
[23] M. Ikeya, *J. Phys. Soc. Jpn.* **1997**, *42*, 168–174.

Manuscript received: May 5, 2023
Revised manuscript received: June 17, 2023
Accepted manuscript online: June 25, 2023
Version of record online: July 5, 2023